

# **Title:** Complex pH-Dependent Interactions Between Weak Polyelectrolyte Block Copolymer Micelles and Molecular Fluorophores

Stacy M. Copp<sup>1,2,3\*</sup>, Ryan L. Hamblin<sup>4†</sup>, Kirstie Swingle<sup>4‡</sup>, Durgesh Rai<sup>5</sup>, Volker Urban<sup>5</sup>, Sergei A. Ivanov<sup>4</sup>, Gabriel A. Montaña<sup>6,7\*</sup>

<sup>1</sup> Department of Materials Science and Engineering, University of California, Irvine, Irvine, CA, 92697-2585, [USA](#)

<sup>2</sup> Department of Physics and Astronomy, University of California, Irvine, Irvine, CA, 92697-4575, [USA](#)

<sup>3</sup> Department of Chemical and Biomolecular Engineering, University of California, Irvine, Irvine, CA, 92697-2580, [USA](#)

<sup>4</sup> Center for Integrated Nanotechnologies, Los Alamos National Laboratories, Los Alamos, NM 87545, [USA](#)

<sup>5</sup> Neutron Scattering Division, Oak Ridge National Laboratory, Oak Ridge, ORNL TN 37830, [USA](#)

<sup>6</sup> Department of Applied Physics and Materials Science, Northern Arizona University, Flagstaff, AZ, 86011, [USA](#)

<sup>7</sup> Center for Materials Interfaces in Research and Applications, Northern Arizona University, Flagstaff, AZ, 86011, [USA](#)

\*Co-corresponding authors: [stacy.copp@uci.edu](mailto:stacy.copp@uci.edu), [Gabriel.Montano@nau.edu](mailto:Gabriel.Montano@nau.edu)

†Current address: Department of Chemistry, The University of Virginia, Charlottesville, Virginia 22904, [USA](#)

‡Current address: School of Molecular Sciences, Arizona State University, Tempe, AZ 85287, [USA](#)

**ABSTRACT:** Amphiphilic block copolymers with weak polyelectrolyte blocks can assemble stimulus-responsive nanostructures and interfaces. Applications of these materials in drug delivery, biomimetics, and sensing largely rely on the well-understood swelling of polyelectrolyte chains upon deprotonation, often induced by changes in pH or ionic strength. This deprotonation can also tune interfacial interactions between the polyelectrolyte blocks and surrounding solution, an effect which is less studied than morphological swelling of polyelectrolytes but can be just as critical for intended function. Here, we investigate whether the pH-driven morphological response of polyelectrolyte-bearing nanostructures also affects the interactions of these nanostructures with molecules in solution, using of micelles of a short-chain polybutadiene-*block*-poly(acrylic acid) (pBd-pAA) as a model system. We introduce a Förster resonance energy transfer (FRET) approach to probe interactions between micelles and fluorescent molecular solutes as a function of solution pH. As expected, the pAA corona of these pBd-pAA micelles increases in thickness monotonically as a function of pH. However, FRET efficiency, which provides a metric of the spatial proximity of fluorescently labeled micelles and freely diffusing fluorophores, exhibits complex nonmonotonic behavior as a function of pH, indicating that the average separation of micelles and acceptor fluorophores is not strictly correlated with micelle swelling. Dialysis experiments quantify the affinity of fluorophores for micelles as a function of pH, confirming that changes in FRET are driven almost entirely by pH-dependent affinity of the pAA block for the investigated molecular fluorophores, not simply by shape change of the pAA corona. This study provides key insights into the interfacial interactions between weak polyelectrolyte-bearing nanostructures and molecular solutes, of importance for the development of their stimulus-responsive applications.

**INTRODUCTION:** Amphiphilic block copolymers (ABCs) are versatile building blocks for responsive nanomaterials. Well-known for assembling a plethora of structures, from solution-phase micelles, vesicles, and tubes<sup>1</sup> to complex films,<sup>2</sup> the morphology of an ABC nanostructure is controlled by copolymer block chemistries and lengths as well as environmental factors such as temperature, solvent composition, and pH. Nanostructures and interfaces formed from stimulus-responsive ABCs can themselves respond to a diverse range of stimuli,<sup>3</sup> such as temperature,<sup>4</sup> pH,<sup>5,6</sup> light,<sup>7</sup> and biomolecular analytes.<sup>8</sup> Predictive design of stimulus-responsive ABC nanomaterials not only requires understanding of stimulus-induced changes in polymer morphology but also if and how such morphological changes tune the interactions of these nanostructures with their local environment.

This study focuses on micelles of a short-chain ABC, polybutadiene-*block*-poly(acrylic acid) (pBd-pAA). Short-chain (low molecular weight) ABCs are of particular interest for their ability to assemble biomimetic polymer membranes,<sup>9,10</sup> hybrid lipid/polymer bilayers,<sup>11</sup> and complex membrane-bound architectures.<sup>12-14</sup> Because integration of stimulus response into these biomimetic materials is highly promising for applications such as controlled release, a comprehensive understanding of the behavior of such stimulus-responsive short-chain ABC nanostructures is necessary.

The hydrophilic block of the ABC studied here is pAA, a weak polyelectrolyte that is well-known for pH-dependent and ionic strength-dependent swelling.<sup>15-17</sup> Below its pKa, when carboxyl groups of pAA are protonated, the polymer chain adopts a compact, globular structure. Upon deprotonation, pAA transitions to an extended coil structure in its charged and fully solvated state.<sup>18,19</sup> The pH dependence of pAA-containing ABCs has been harnessed for responsive materials such as nanoporous films with pH-tuned porosity,<sup>20</sup> color-switching plasmonic films,<sup>21</sup>

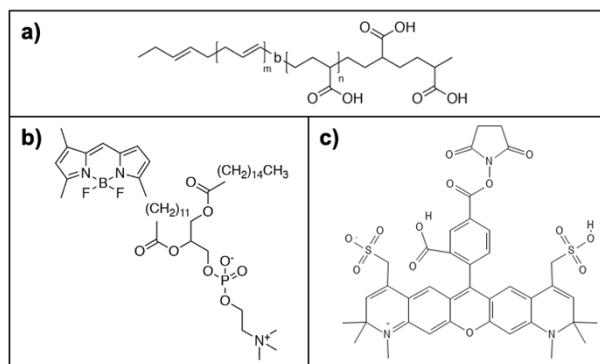
and polymersomes with pH-tuned shape change<sup>22</sup> and/or controlled release.<sup>23</sup> Each of these applications capitalizes on morphological change of pAA driven by its weak polyelectrolyte behavior. (We note that there is interesting controversy over the effect of pAA chain length on the pH response of solution-phase pAA at low molecular weights;<sup>18,24,25</sup> because the present study concerns pAA incorporated into an ABC micelle, we do not comment further on this controversy.) While much attention has been paid to the shape change of pAA-incorporating nanostructures resulting from electrostatic repulsion of pAA chains, pAA deprotonation may also alter the interfacial interactions of pAA-bearing colloids with other molecules in solution, meaning that shape change in pAA-incorporating nanostructures would not be an inert process which simply alters morphology alone. pAA has well-established propensity to complex with other macromolecules, especially due to hydrogen bonding in its neutral state.<sup>26–28</sup> Such charge-driven interactions between pAA and molecular solutes could affect applications of pAA to control cargo release<sup>23</sup> or gate the flow of small molecules or macromolecules,<sup>20</sup> meaning that solution pH or ion composition could have a nontrivial effect on the functional response of pAA-based nanomaterials.

To explore the roles of morphological change *versus* degree of protonation in tuning properties of pAA-based nanomaterials, we study the interactions of pBd-pAA micelles with small molecules and macromolecules in buffered aqueous solution as a function of pH. To monitor the interfacial interactions of micelles with solute molecules, we harness the process of Förster resonance energy transfer (FRET), whereby energy from an excited “donor” fluorophore nonradiatively transfers to an “acceptor” fluorophore.<sup>29</sup> Efficiency of this process,  $E_{FRET}$ , scales strongly with nanoscale separation of donor and acceptor (Equation 1), making FRET a commonly used indicator of nanoscale proximity in biology,<sup>30,31</sup> biosensing technologies,<sup>32,33</sup> and

fundamental studies of solution-phase polymers.<sup>34</sup> We incorporate a low concentration of amphiphilic donor fluorophores into pBd-pAA micelles and monitor  $E_{FRET}$  between micelles and free acceptor fluorophores in solution, including unfunctionalized acceptor fluorophores and acceptor-labeled macromolecules. Dynamic light scattering and small angle neutron scattering experiments confirm that pBd-pAA micelle radius increases monotonically as pH increases, with maximal rate of expansion near the expected pKa of pAA. However,  $E_{FRET}$  exhibits nonmonotonic behavior as a function of pH, in contrast to what is expected if increasing pH correlates with increasing distance between the micelle-associated donor and solution-suspended acceptors due to steric repulsion between fluorophores and pAA chains. To probe whether this complex behavior arises from pH-tuned affinity of pAA with the fluorophore solutes, we compare  $E_{FRET}$  to the relative affinity of acceptor fluorophores for pBd-pAA micelles by measuring the “membrane interaction factor” (MIF) as introduced by Hughes, *et al.*<sup>35</sup> Trends of MIF and  $E_{FRET}$  with pH agree well for both small molecule acceptor fluorophores and fluorophore-labeled macromolecules. These results support that swelling of surface-bound or nanostructure-bound weak polyelectrolyte interfaces cannot *a priori* be assumed to act as passive shape change elements. Rather, other pH-dependent interactions of pAA with solute molecules may play a nonnegligible role in interactions between solution phase and pAA domain.

**EXPERIMENTAL METHODS:** *Materials:* Poly(1,4-butadiene)-*block*-poly(acrylic acid) (pBd-pAA) with 1.0 kDa pBd and 2.2 kDa pAA and a polydispersity index of 1.3 was purchased from Polymer Source Inc.  $\beta$ -BODIPY FL C12-HPC ((2-(4,4-Difluoro-5,7-Dimethyl-4-Bora-3a,4a-Diaza-*s*-Indacene-3-Dodecanoyl)-1-Hexadecanoyl)-*sn*-Glycero-3-Phosphocholine), Alexa Fluor 594 C5 maleimide, and 10 kDa Dextran labeled with Alexa Fluor 594 were purchased from

ThermoFisher Scientific. 2 kDa polyethylene glycol (PEG) labeled with Alexa Fluor 594 was purchased from Nanocs. Chemical structures for pBd-pAA,  $\beta$ -BODIPY FL C12-HPC, and Alexa Fluor 594 are given in Scheme 1. Water infusion was performed in molecular biology reagent-grade water (Sigma Aldrich). Scattering and spectroscopy experiments were performed in phosphate/citrate buffer at varying pH values (see Table S1 in Supporting Information), prepared using trisodium citrate dihydrate and disodium hydrogen phosphate in molecular biology reagent-grade water at 0.9 M total ionic strength. This buffer was chosen to ensure sufficient buffer capacity<sup>36</sup> within the target pH range, with the expected variation in pH an order of magnitude below measurement precision for the charged species concentrations of the pAA at the minimally buffered pH. Low-retention pipette tips were used to prepare all samples for highly accurate volume control.



**Scheme S1:** Chemical structures of poly(1,4-butadiene)-*block*-poly(acrylic acid) (pBd-pAA), BODIPY FL donor fluorophore conjugated to C12-HPC lipid, and Alexa Fluor 594 acceptor fluorophore.<sup>37</sup>

*Micelle self-assembly:* pBd-pAA and BODIPY-HPC were separately dissolved in THF, and a 500  $\mu$ L solution of 5 mM pBd-pAA and 12.5  $\mu$ M BODIPY-HPC in THF was then mixed in a scintillation vial. The uncapped solution was stirred at 700 rpm with a flea-sized stirbar during infusion with 2.5 mL of water at a rate of 2 mL/hr, while protecting from light. After water infusion, the solution was allowed to stir overnight to allow THF to evaporate from solution, after

which no THF vapors were detectable. Note: this process was carried out in a fume hood at room temperature to ensure chemical safety. (Dynamic light scattering (DLS) showed that micelles formed by gentle rotary evaporation immediately after water infusion possess diameters equal to the passive evaporation method. However, because micelles prepared by rotary evaporation occasionally aggregated significantly, we use only micelles by the passive evaporation method for the studies here.) Solutions were returned to 2.5 mL total volume by addition of water and filtered three times using a 0.2  $\mu\text{m}$  syringe filter. Micelles formed without BODIPY-HPC were formed using the same process but with no BODIPY-HPC added.

*Light scattering:* Static light scattering (SLS) and DLS were performed on a Zetasizer Nano ZS (Malvern Instruments) equipped with a 633 nm laser. For SLS, various dilutions of micelles without BODIPY-HPC were mixed in volumetric flasks, and quartz cuvettes were washed three times with each micelle solution prior to sample measurement. Using various concentrations of pBD-pAA micelles in water,  $dn/dc$  was measured to be  $0.15 \pm 0.03$  g/mL using an Abbe-3L refractometer (Bausch & Lomb). For DLS, a 500  $\mu\text{L}$  sample solution of 0.2 mM pBD-pAA micelles in phosphate/citrate buffer was mixed in single-use PMMA cuvettes. Samples were prepared at pH values from pH 3 to pH 7 in half integer steps.

*Fluorescence spectroscopy:* Sample solutions of 500  $\mu\text{L}$  of 0.2 mM pBD-pAA micelles, with BODIPY-HPC were prepared with and without acceptor fluorophores in single-use PMMA cuvettes in pH-controlled phosphate/citrate buffer. Samples were prepared at pH values from pH 3 to pH 7 in half integer steps. UV-Vis absorption spectra for each sample were obtained on a Cary 6000i spectrometer. Fluorescence emission spectra for all samples were collected by 450 nm excitation using a PTI fluorimeter. FRET efficiency  $E_{FRET}$  was determined at each pH value using Eq. 2, with intensity in the presence and absence of acceptor ( $I_D$  and  $I_{DA}$ , respectively) represented

by integrated intensity of the donor spectrum from 500 nm to 570 nm (this range excludes any appreciable emission from A594).

*MIF experiments:* pBD-pAA micelles were prepared with BODIPY-HPC as described above. 100  $\mu\text{L}$  of 0.2 mM pBD-pAA micelles and acceptor fluorophore in pH controlled phosphate/citrate buffer was placed in ThermoFisher Scientific 10 kDa MWCO MINI Dialysis Units. Dialysis units were suspended in 1400  $\mu\text{L}$  of acceptor fluorophore of the same concentration as the micelle-containing sample, sealed with parafilm, and incubated in the dark at 4  $^{\circ}\text{C}$  on a rotation table at 0.01 RCF for  $\sim$ 72 hours. After incubation, 50  $\mu\text{L}$  of the solution within the dialysis unit and 50  $\mu\text{L}$  of solution outside the dialysis unit were each mixed via pipetting with 450  $\mu\text{L}$  of phosphate/citrate buffer in single-use PMMA cuvettes. Samples were prepared at pH values from pH 3 to pH 7 in half integer steps. Emission spectra for each sample were recorded at two excitation wavelengths, 450 nm and 580 nm. Spectra at 450 nm were used to confirm that micelles remained inside the dialysis units *via* the intensity of the BODIPY FL. Spectra at 580 nm were used to determine the emission intensity of the acceptor fluorophore for MIF calculations. All emission spectra were recorded on a PTI fluorimeter.

*Small angle neutron scattering (SANS):* SANS<sup>38</sup> was performed using the CG-3 Bio-SANS instrument<sup>39</sup> on pBd-pAA micelles at 0.27 mass % in 100% D<sub>2</sub>O, at pH 3 and pH 6 (Figure S4). Measurement and data analysis followed approaches as in our preceding work, described elsewhere.<sup>10</sup> A core-shell sphere model accounting for polydispersity was used to analyze SANS data, with details provided in Supporting Information.

**RESULTS AND DISCUSSION:** Micelles of pBd-pAA with molecular weights (MWs) of 1 kDa pBd and 2.2 kDa pAA (approximately corresponding to pBd<sub>18</sub>-pAA<sub>31</sub>) were prepared by slow

infusion of ultrapure water into a stirred solution of pBd-pAA dissolved in tetrahydrofuran (THF), followed by passive evaporation of residual THF under constant stirring at room temperature (details in Experimental Methods). Micelles were measured to have a MW of  $980 \pm 30$  kDa by static light scattering (SLS), corresponding to an aggregation number of  $306 \pm 9$  polymers per micelle (Figure S2).

To test the effect of pH on micelle size, a series of micelle solutions were prepared by dilution in phosphate-citrate buffers of controlled pH. The buffer was designed to ensure that no change in solution pH is expected to within measurement error for micelle solutions over the entire pH range studied here (details in Materials and Methods.) DLS shows that micelle radius increases about 40% as buffer pH increases from 3 to 7 (Figure 1), with maximal rate of increase near pH 4.5, which is the expected pKa of linear pAA that is free in solution.<sup>18</sup> pH-dependent responses of weak polyelectrolytes are known to be influenced by steric effects, such as confinement to a nanoparticle surface or structural constraints on nonlinear polymers.<sup>40-42</sup> Consistent with these past studies, we find that micelle radius increases over a larger pH range than is observed for solvated linear pAA chains alone.<sup>40</sup>

We confirmed the change in micelle radius by SANS. SANS shows an effective radius increase of 38% between pH 3 and 6, caused almost entirely by expansion of the pAA micelle corona, while the pBd core remains largely unchanged (Table 1). Thus, it is reasonable to conclude that pH-dependent swelling of pBd-pAA micelles is due to pAA expansion upon deprotonation, with increasing repulsion of individual pAA chains in the micelle corona as they acquire net negative charge.<sup>18,19</sup> We note that zeta potential measurements were prohibited by extreme aggregation of our samples during measurement. This instability may result, in part, from pBd's

low glass transition temperature,  $T_g$ , enabling facile rearrangement of micelles under external stimulus.

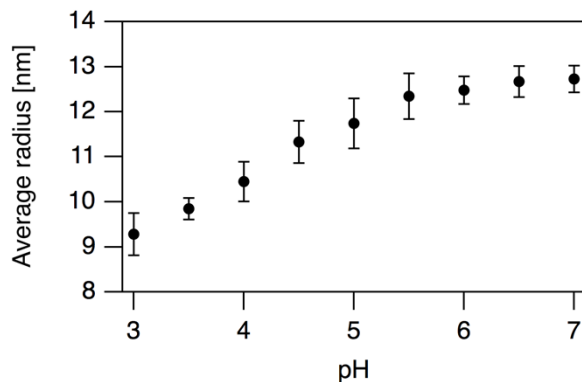


**Figure 1:** Average radius of pBD-pAA micelles in phosphate-citrate buffer of varying pH, as measured by DLS. Reported values and standard deviations are for the intensity distribution (see Figure S3 for volume distribution) and are averaged from eight separate trials.

pH	Core radius (nm)	Shell thickness (nm)	Effective radius (nm)	Polydispersity index
pH 6	6.33±0.01	8.4±0.1	14.8±0.1	0.14±0.01
pH 3	6.04±0.03	4.7±0.1	10.7±0.1	0.20±0.01

**Table 1:** Small angle neutron scattering studies of pBD-pAA micelles (0.27% weight/weight in pH-controlled H<sub>2</sub>O) as a function of pH. Raw data provided in Figure S4.

We next studied the pH-tuned interactions of these micelles with molecular solutes. Specifically, we employed FRET between donor fluorophores embedded within the micelles and acceptor fluorophores free in solution. Förster theory describes FRET efficiency,  $E_{FRET}$ , as a function of the separation of donor and acceptor molecules,  $r$ .<sup>43,44</sup>

$$E_{FRET}(r) = 1/[1 + (r/R_0)^6] \quad (1)$$

$R_0$  is the separation of donor and acceptor at which  $E_{FRET}(R_0) = 0.5$  and is a function of donor fluorescence quantum yield, acceptor extinction coefficient, spectral overlap of donor and acceptor, and relative angular orientation of donor and acceptor (see Supporting Information). For ideal pairs of donor and acceptor fluorophores, typical values of  $R_0$  are 5-8 nm.<sup>31</sup>  $E_{FRET}$  may be

determined by steady-state fluorimetry from fluorescence intensity of the donor fluorophores in the absence of the acceptor,  $I_D$ , and the presence of the acceptor,  $I_{DA}$ :

$$E_{FRET}(r) = 1 - I_{DA}/I_D \quad (2)$$

Equation (2) is valid when all donors are paired with acceptors.<sup>29</sup>

Donor fluorophores are embedded within micelles using a phosphocholine lipid with a BODIPY FL chromophore attached *via* a C<sub>12</sub>-fatty acyl chain (BODIPY FL-HPC). BODIPY FL is favorable for its high extinction coefficient and quantum yield, stability, and low tendency to aggregate. BODIPY-HPC can be embedded at low mole fractions within the hydrophobic core of low MW poly(ethylene oxide)-pBd micelles without altering micelle structure.<sup>9,10</sup> BODIPY-HPC was added to THF-dissolved pBd-pAA at 0.25% mol/mol ratio of BODIPY:pBd-pAA, followed by water infusion to induce micelle assembly. To avoid self-quenching of multiple BODIPY FL fluorophores, this 0.25% mol/mol ratio was chosen to ensure that, on average, micelles contain less than one BODIPY-HPC. (Using the SLS-determined aggregation number of the pBD-pAA micelles, each micelle contains ~0.8 BODIPY-HPC on average.)

Fluorescence emission spectra of BODIPY FL-containing micelles show that BODIPY FL spectral shape is constant for buffer pH from 3 to 7. Increased pH causes a slight  $8 \pm 3\%$  increase in peak BODIPY FL emission intensity (Figure S5), perhaps due to subtle rearrangement of the polymer in the local vicinity of the fluorophore. We account for this small change in BODIPY FL fluorescence intensity by using a separate control sample at each pH condition for measurement of  $I_D$  (donor intensity in the absence of acceptor fluorophore, as in Eq. 1 for  $E_{FRET}$ ).

We selected Alexa Fluor 594 (A594) as a FRET acceptor.<sup>37</sup> Emission spectra of A594 and BODIPY FL have minimal overlap, reducing donor and acceptor crosstalk, yet maintain sufficient spectral overlap of donor emission with acceptor excitation as needed for FRET (Figure 2a). The

A594 derivative chosen (Materials and Methods) is water-soluble and pH-insensitive over a wide pH range. Figure 2b shows calculated FRET efficiency,  $E_{FRET}$ , for BODIPY FL and A594 plotted as a function of fluorophore separation (calculation using Eq. S1 in Supporting Information). Because donor and acceptor are separated by a mixture of water ( $n = 1.333$ ) and pAA ( $n \approx 1.5$ ), the exact refractive index of the separating medium is unknown. We report calculated values for medium refractive index of both water and pAA, estimating  $R_0 = 5.0 - 5.5$  nm. Thus, the length scale of greatest change in  $E_{FRET}$  occurs for donor-acceptor separations comparable to the pAA shell thickness determined by SANS, making A594 and BODIPY-FL a favorable FRET pair for this study. Further, we confirmed that A594 is spectrally stable to pH changes, with a slight shift in A594 absorbance spectrum from pH 3 to pH 7 resulting in an increase of calculated  $R_0$  value by 4% (Figure S6). This small increase does not prohibit monitoring changes in separation between donor and acceptor using  $E_{FRET}$ .

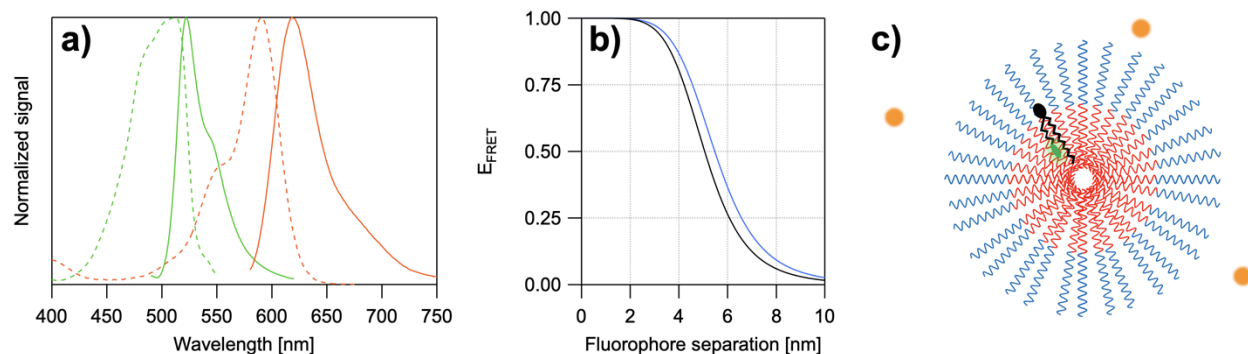


**Figure 2:** **a)** Normalized donor (green) and acceptor (red) excitation (dashed) and emission (solid) spectra. **b)** FRET efficiency  $E_{FRET}$  calculated for refractive indices of water (blue) and polymer (black). **c)** Schematic (not to scale) of pBD-pAA micelle containing BODIPY FL donor and A594 acceptor reporters. Micelles contain an average of 0.8 donor fluorophore (black and green) buried in the hydrophobic polymer blocks (red). Acceptor molecules (orange spheres) are free in aqueous solution surrounding the hydrophilic micelle corona (blue). At chosen concentrations, there are approximately 2-3 acceptors per micelle.

Next, we test how pH-induced expansion of pAA alters the average separation between the micelle-embedded BODIPY FL donor and freely solvated A594 acceptors. Fig. 2c illustrates

presumed positions of donor within the hydrophobic micelle core and acceptors diffusing freely in solution. At the concentrations used here, there is an average of  $\ll 1$  donor per micelle and 2-3 acceptors per micelle. The simplest assumption is that A594 molecules randomly distribute in solution because no specific interaction between the A594 and pAA corona is expected at the relatively mild pH values studied here. If acceptor fluorophores are excluded from the pAA corona by steric hindrance as the corona swells, we expect an inverse correlation of  $E_{FRET}$  with micelle radius. Note that the value of  $E_{FRET}$  is measured in bulk solution, representing the average of all FRET efficiencies of individual pairs of BODIPY-FL and A594.

$E_{FRET}$  was measured for pH values from 3 to 7, using  $I_D$  and  $I_{DA}$  determined by integrated intensity of BODIPY FL fluorescence emission spectrum. A594 concentration was selected to ensure  $E_{FRET}$  values above 0.25 for highest sensitivity to changes in donor-acceptor separation, corresponding to 1.4  $\mu\text{M}$  A594 in a solution of 200  $\mu\text{M}$  pBd-pAA; this corresponds to  $\sim 2$  A594 molecules per micelle. Figure 3a shows that polydispersity index (PDI) of micelle solutions remains low for all pH values, precluding any significant aggregation. Surprisingly, we found that  $E_{FRET}$  varied nonmonotonically with increasing pH (Figure 3b). The same behavior was observed for a second acceptor dye, Alexa 647 (Figure S7). When acceptor fluorophores were instead embedded within the micelle core, using Texas Red 1,2-Dihexadecanoyl-*sn*-Glycero-3-Phosphoethanolamine (DHPE),  $E_{FRET}$  remained constant to within experimental error across the pH range tested (Figure S8), which is expected given the negligible change of the pBd micelle core found by SANS and supporting that variation in  $E_{FRET}$  for A594 arises from pH-dependent changes to the pAA corona. However, Figure 3b is inconsistent with a model in which acceptor fluorophores are randomly distributed in solution and are excluded from the swelling micelle corona. Furthermore, while pAA has well-known propensity to form molecular complexes with

macromolecules, especially at low pH,<sup>26,27,45</sup> Figure 3a precludes any significant micelle aggregation.

We consider two possible mechanisms for the nonmonotonicity of  $E_{FRET}$  with pH: either (i) A594 is attracted to the deprotonated, charged pAA or (ii) A594 molecules *passively* diffuse into the pAA corona as pAA chains elongate and the corona's water content increases, thus reducing average distance between BODIPY-FL and A594 fluorophores. To investigate the latter case, we calculate the increase in pAA corona volume upon swelling at high pH (details in Supporting Information Note 1). Using dimensions determined by SANS (Table 1, Figure S4) and assuming that A594 concentration in the swollen pAA corona is equal to bulk A594 concentration (*i.e.* no specific interactions exist between A594 and pAA), an additional 0.007 A594 molecules is expected, on average, to enter the micelle corona upon swelling from pH 3 to pH 6. These additional A594 would result in a negligible average increase in A594 proximity to BODIPY-FL, which cannot alone explain the large  $\sim 40\%$  increase in  $E_{FRET}$  from pH 5 to pH 6. Thus, it is plausible that there exists a separate pH-dependent attraction between A594 and the deprotonated pAA corona.

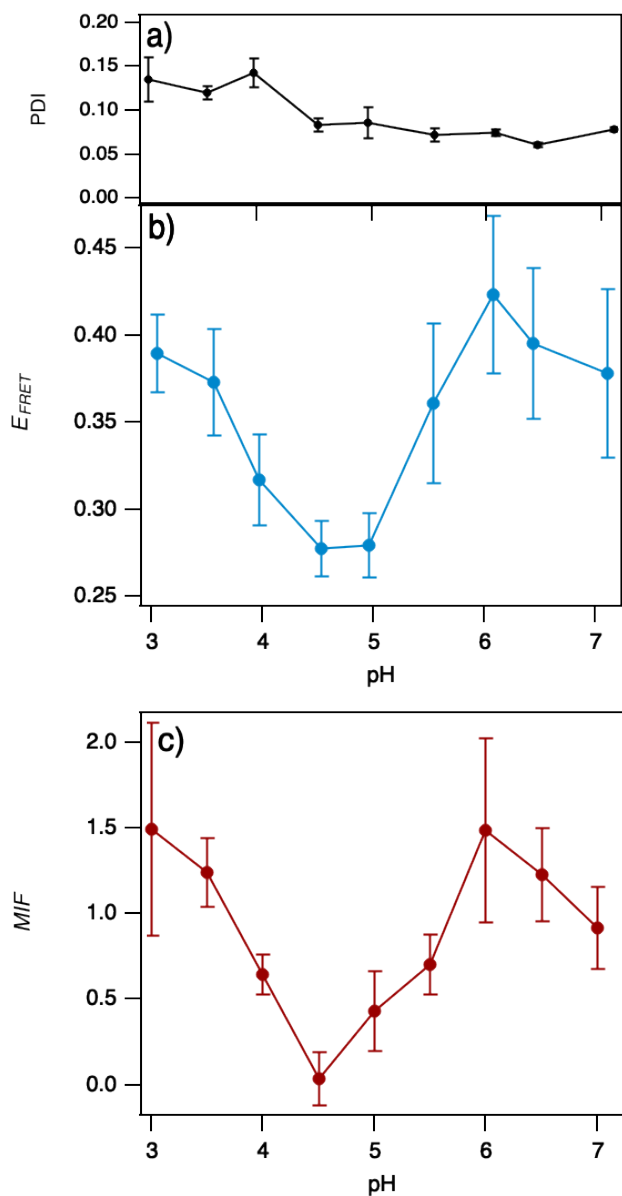


**Figure 3:** **a)** Polydispersity index (PDI) and **b)**  $E_{FRET}$  as determined by Eq. 1 for solutions of 200  $\mu\text{M}$  pBd-pAA (assembled into micelles with embedded BODIPY-FL) and 1.4  $\mu\text{M}$  A594 in phosphate-citrate buffer of varying pH. **c)** MIF for solutions of 200  $\mu\text{M}$  pBd-pAA (assembled into micelles with embedded BODIPY-FL) and 2  $\mu\text{M}$  A594 in phosphate-citrate buffer of varying pH. All data points and standard deviation error bars in graphs determined by triplicate experiments.

To probe the existence of a pH-dependent interaction between A594 and pBd-pAA micelles, we adapted an approach by Hughes, *et al.*, to quantify fluorophore affinity for lipid vesicles.<sup>35</sup> pBd-pAA micelles are placed into a dialysis cup with a 10 kDa MW cutoff (MWCO)

chosen to restrict micelles to within the dialysis cup while allowing A594 to freely diffuse across the dialysis membrane. Solutions inside and outside the dialysis cup are prepared with equal concentrations of A594 and incubated under gentle shaking for ~72 hours at 4°C (refrigeration protects BODIPY-HCP from degradation; full details in Methods). If A594 has no specific affinity for the micelles, the concentrations of A594 inside and outside the dialysis cup will remain equal. However, if A594 does have an affinity for micelles, A594 will concentrate within the dialysis cup over time. Hughes, *et al.*, defined the Membrane Interaction Factor (*MIF*) to quantify relative imbalance in fluorophore concentration in terms of fluorophore intensity inside the dialysis cup,  $I_{in}$ , and outside the cup,  $I_{out}$ :

$$MIF = \frac{I_{in} - I_{out}}{I_{out}} = \frac{I_{in}}{I_{out}} - 1 \quad (3)$$

To account for the possibility of incomplete fluorophore equilibration across the dialysis membrane,<sup>35</sup> we also performed experiments in the absence of micelles for all acceptor fluorophores studied here, finding  $MIF \approx 0$  as expected for these fluorophores (Figure S9). Thus, Equation 3 is used as stated.<sup>35</sup> To improve sensitivity of measurements to slight changes in A594 concentration, we increased A594 concentration to 2  $\mu$ M for *MIF* experiments. Solutions outside of the dialysis cup were screened for residual BODIPY fluorescence, and the few leak-associated samples were rejected from averages reported here.

Figure 3c shows average *MIF* values measured for solutions of pBd-pAA micelles and A594 from pH 3 to pH 7. Comparison of Figures 3b and 3c shows marked similarities between trends for *MIF* and  $E_{FRET}$ : both quantities decrease with increasing pH until pH 4.5 to 5, followed by an increase until pH 6 and a leveling off or decrease at and above pH 6.5. This strongly suggests that the main driver of pH-dependent trend of  $E_{FRET}$  is not morphological change in the micelle corona but rather a deprotonation-driven attraction of pAA and A594 fluorophores. (Because *MIF*

varies as a function of pH, A594 concentration is not constant at all pH values; thus,  $E_{FRET}$  values measured for *MIF* experiments are not directly comparable to one another and are not reported here.)

We next explored whether bulkier macromolecules are excluded from the deprotonated pAA corona due to increased steric hindrance. pH-dependent expansion of pAA has been used to selectively open and close nanoscale pores within a membrane, suggesting the possibility of such an effect.<sup>20</sup>  $E_{FRET}$  and *MIF* were measured in triplicate for fluorophore-labeled polyethylene glycol (PEG) and dextran, using higher MWCO dialysis membranes of 20 kDa. While PEG was chosen due to its inert nature, we found that even when no micelles were present, fluorophore-labeled PEG dramatically concentrated within the dialysis membranes in a non-pH dependent manner, preventing statistically significant measurement of *MIF* values when micelles were present. Thus, we only report  $E_{FRET}$  and *MIF* for A594-labeled dextran, which did not possess the same aggregation behavior as PEG (Figure S9). We found that  $E_{FRET}$  exhibited a sudden increase at pH 5.5, and this increase corresponded directly to an increase in *MIF* (Figure 4). This suggests that for A594-labeled dextran, pH-specific attraction to pAA is also the main driving force of proximity to the micelle core, rather than steric hindrance-induced changes due to swelling of the micelle corona. Given the complexity of dextran macromolecules, such an attraction could be reasonably expected.

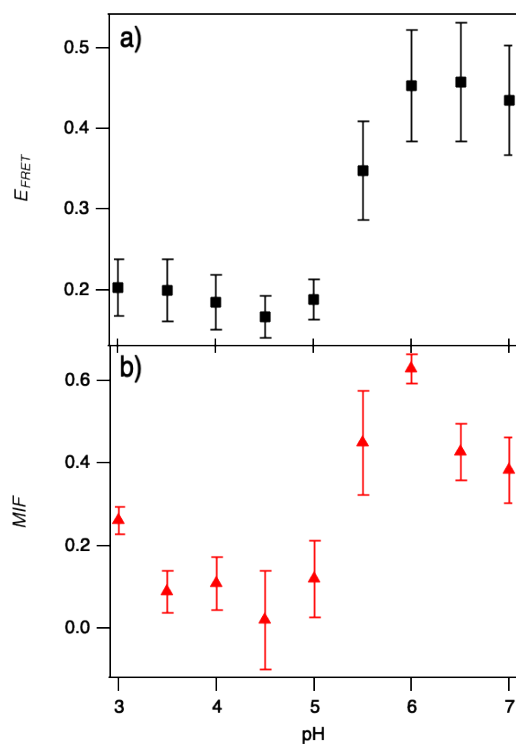


**Figure 4:** **a)**  $E_{FRET}$  and **b)**  $MIF$  measured for solutions of 200  $\mu\text{M}$  pBd-pAA (in micelle form) and 2  $\mu\text{M}$  A594-dextran. All data points and standard deviation error bars in graphs determined by triplicate experiments.

This study shows that ABC nanostructures with pAA interfaces can have surprising and complex affinity for molecular fluorophores, and this affinity plays a much more significant role in controlling pAA-molecule interactions than steric effects from expansion of pAA blocks. Given the complex behavior of weak polyelectrolytes and their coacervates,<sup>46</sup> such behavior is not unexpected. For example, turbidimetry of solutions of the protein bovine serum albumin (BSA) and pAA shows nonmonotonic pH-dependent interactions between BSA and pAA, with onset of BSA-pAA complexation at pH 3 and decomplexation at pH 4.5. This effect was attributed to electrostatic interactions between BSA and pAA.<sup>40</sup> However, our studies here are performed at much higher ionic strengths than the studies in Ref. 40, as our buffer system was chosen to screen possible electrostatic attractions. This may preclude electrostatic interactions as the main source

of the pAA-fluorophore interaction we observe, with ionic strength-insensitive Van der Waals interactions<sup>47</sup> possibly dominating the observed behavior. While a full determination of the exact mechanisms for the pH-driven attractions we observe are outside of the scope of this study, our results show that care should be taken to ensure that these types of pH-dependent interactions of weak polyelectrolyte interfaces with molecular solutes are not misinterpreted for ABC-biological interfaces or biomimetic applications. Furthermore, molecular fluorophores and fluorophore-conjugated macromolecules are ubiquitous in the biosciences. Thus, as low-molecular weight ABCs continue to find applications as lipid mimics for formation of biomimetic membranes and architectures,<sup>9,11,23</sup> it will be increasingly important to understand the interfacial interactions of such ABC membranes with fluorophores, and in particular for membranes which incorporate weak polyelectrolytes.

**CONCLUSIONS:** We report a fluorescence-based experimental method to probe the molecular interactions of short-chain ABC micelles with pAA hydrophilic blocks and solute fluorophores. While DLS and SANS show that the micelle's pAA corona swells with increasing solution pH, FRET experiments show that this expansion does not simply drive solute fluorophores further from the micelle core. Rather, by a series of dialysis experiments, we find that FRET efficiency is correlated strongly with the pH-dependent molecular affinity of the micelle's pAA interface for both small molecule fluorophores and their macromolecular conjugates. The presented study provides a sensitive method to screen for possible solution-dependent interfacial interactions of ABC nanostructures and fluorophore-labeled molecules and emphasizes that weak polyelectrolyte blocks are not inert shape-changing agents but that their degree of protonation can drive complex

interactions with surrounding solutes. This study also demonstrates the utility of combining FRET and MIF measurements for elucidating interfacial interactions.

***Supporting Information Description:*** The Supporting Information is available free of charge at [to be assigned].

- Data and model details for light scattering and SANS experiments to determine micelle molecular weight and dimensions
- Equations for FRET length, buffer composition table, and calculation of micelle corona expansion volume
- pH dependence of fluorescence spectra of donor alone and acceptor alone, FRET efficiency as a function of pH for additional acceptor dyes, and MIF factors for acceptor dyes in absence of micelles

***Acknowledgements:*** The authors acknowledge financial support by the Laboratory Directed Research and Development (LDRD) program and the use of the jMIRA! core facilities at Northern Arizona University supported in part by ECCS-2025490. S.M.C. acknowledges support for materials costs from a University of California President's Postdoctoral Fellowship and a L'Oreal USA for Women in Science Fellowship. Neutron scattering research conducted at the Bio-SANS instrument, a DOE Office of Science, Office of Biological and Environmental Research Structural Biology Resource. This research used resources at the High Flux Isotope Reactor, DOE Office of Science, Scientific User Facilities operated by the Oak Ridge National Laboratory (ORNL). This work was performed, in part, at the Center for Integrated Nanotechnologies, an Office of Science User Facility operated for the U.S. Department of Energy (DOE) Office of Science by Los Alamos

National Laboratory (Contract 89233218CNA000001) and Sandia National Laboratories (Contract DE-NA-0003525). A portion of this research used resources at the Spallation Neutron Source, a DOE Office of Science User Facility operated by the Oak Ridge National Laboratory.

### ***ORCID IDs***

Stacy M. Copp: 0000-0002-1788-1778

Durgesh K. Rai: 0000-0001-7257-7210

Volker Urban: 0000-0002-7962-3408

Sergei A. Ivanov: 0000-0001-6790-5187

Gabriel A. Montaña: 0000-0001-5074-8736

### ***References:***

- (1) Mai, Y.; Eisenberg, A. Self-Assembly of Block Copolymers. *Chem. Soc. Rev.* **2012**, *41* (18), 5969. <https://doi.org/10.1039/c2cs35115c>.
- (2) Kempe, K.; Killops, K. L.; Poelma, J. E.; Jung, H.; Bang, J.; Hoogenboom, R.; Tran, H.; Hawker, C. J.; Schubert, U. S.; Campos, L. M. Strongly Phase-Segregating Block Copolymers with Sub-20 Nm Features. *ACS Macro Lett.* **2013**, *2* (8), 677–682. <https://doi.org/10.1021/mz400309d>.
- (3) Theato, P.; Sumerlin, B. S.; O'Reilly, R. K.; Epps, III, T. H. Stimuli Responsive Materials. *Chem. Soc. Rev.* **2013**, *42* (17), 7055. <https://doi.org/10.1039/c3cs90057f>.
- (4) Gibson, M. I.; O'reilly, R. K. To Aggregate, or Not to Aggregate? Considerations in the Design and Application of Polymeric Thermally-Responsive Nanoparticles. *Chem. Soc. Rev.* **2013**, *42* (17), 7204–7213. <https://doi.org/10.1039/c3cs60035a>.
- (5) Rodríguez-Hernández, J.; Lecommandoux, S. Reversible Inside-out Micellization of PH-

- Responsive and Water-Soluble Vesicles Based on Polypeptide Diblock Copolymers. *J. Am. Chem. Soc.* **2005**, *127* (7), 2026–2027. <https://doi.org/10.1021/ja043920g>.
- (6) Kocak, G.; Tuncer, C.; Bütün, V. PH-Responsive Polymers. *Polym. Chem.* **2017**, *8* (1), 144–176. <https://doi.org/10.1039/C6PY01872F>.
- (7) Bertrand, O.; Gohy, J.-F. Photo-Responsive Polymers: Synthesis and Applications. *Polym. Chem.* **2017**, *8* (1), 52–73. <https://doi.org/10.1039/C6PY01082B>.
- (8) Kelley, E. G.; Albert, J. N. L.; Sullivan, M. O.; Epps, III, T. H. Stimuli-Responsive Copolymer Solution and Surface Assemblies for Biomedical Applications. *Chem. Soc. Rev.* **2013**, *42* (17), 7057. <https://doi.org/10.1039/c3cs35512h>.
- (9) Goertz, M. P.; Marks, L. E.; Montaña, G. A. Biomimetic Monolayer and Bilayer Membranes Made from Amphiphilic Block Copolymer Micelles. *ACS Nano* **2012**, *6* (2), 1532–1540. <https://doi.org/10.1021/nn204491q>.
- (10) Adams, P. G.; Collins, A. M.; Sahin, T.; Subramanian, V.; Urban, V. S.; Vairaprakash, P.; Tian, Y.; Evans, D. G.; Shreve, A. P.; Montaña, G. A. Diblock Copolymer Micelles and Supported Films with Noncovalently Incorporated Chromophores: A Modular Platform for Efficient Energy Transfer. *Nano Lett.* **2015**, *15* (4), 2422–2428. <https://doi.org/10.1021/nl504814x>.
- (11) Lim, S.; de Hoog, H.-P.; Parikh, A.; Nallani, M.; Liedberg, B. Hybrid, Nanoscale Phospholipid/Block Copolymer Vesicles. *Polymers (Basel)*. **2013**, *5* (3), 1102–1114. <https://doi.org/10.3390/polym5031102>.
- (12) Collins, A. M.; Timlin, J. A.; Anthony, S. M.; Montaña, G. A. Amphiphilic Block Copolymers as Flexible Membrane Materials Generating Structural and Functional Mimics of Green Bacterial Antenna Complexes. *Nanoscale* **2016**, *8* (32), 15056–15063.

<https://doi.org/10.1039/C6NR02497A>.

- (13) Orf, G. S.; Collins, A. M.; Niedzwiedzki, D. M.; Tank, M.; Thiel, V.; Kell, A.; Bryant, D. A.; Montaña, G. A.; Blankenship, R. E. Polymer–Chlorosome Nanocomposites Consisting of Non-Native Combinations of Self-Assembling Bacteriochlorophylls. *Langmuir* **2017**, *33* (25), 6427–6438. <https://doi.org/10.1021/acs.langmuir.7b01761>.
- (14) Watt, J.; Collins, A. M.; Vreeland, E. C.; Montano, G. A.; Huber, D. L. Magnetic Nanocomposites and Their Incorporation into Higher Order Biosynthetic Functional Architectures. *ACS Omega* **2018**, *3* (1), 503–508. <https://doi.org/10.1021/acsomega.7b02031>.
- (15) Shefer, A.; Grodzinsky, A. J.; Prime, K. L.; Busnel, J. P. Novel Model Networks of Poly(Acrylic Acid): Synthesis and Characterization. *Macromolecules* **1993**, *26* (19), 5009–5014. <https://doi.org/10.1021/ma00071a004>.
- (16) Katchalsky, A.; Eisenberg, H. Molecular Weight of Polyacrylic and Polymethacrylic Acid. *J. Polym. Sci.* **1951**, *6* (2), 145–154. <https://doi.org/10.1002/pol.1951.120060202>.
- (17) Guo, X.; Ballauff, M. Spherical Polyelectrolyte Brushes: Comparison between Annealed and Quenched Brushes. *Phys. Rev. E* **2001**, *64* (5), 051406. <https://doi.org/10.1103/PhysRevE.64.051406>.
- (18) Swift, T.; Swanson, L.; Geoghegan, M.; Rimmer, S. The PH-Responsive Behaviour of Poly(Acrylic Acid) in Aqueous Solution Is Dependent on Molar Mass. *Soft Matter* **2016**, *12* (9), 2542–2549. <https://doi.org/10.1039/C5SM02693H>.
- (19) Laguecir, A.; Ulrich, S.; Labille, J.; Fatin-Rouge, N.; Stoll, S.; Buffle, J. Size and PH Effect on Electrical and Conformational Behavior of Poly(Acrylic Acid): Simulation and Experiment. *Eur. Polym. J.* **2006**, *42* (5), 1135–1144.

<https://doi.org/10.1016/j.eurpolymj.2005.11.023>.

- (20) Weidman, J. L.; Mulvenna, R. A.; Boudouris, B. W.; Phillip, W. A. Unusually Stable Hysteresis in the PH-Response of Poly(Acrylic Acid) Brushes Confined within Nanoporous Block Polymer Thin Films. *J. Am. Chem. Soc.* **2016**, *138* (22), 7030–7039. <https://doi.org/10.1021/jacs.6b01618>.
- (21) Liu, L.; Aleisa, R.; Zhang, Y.; Feng, J.; Zheng, Y.; Yin, Y.; Wang, W. Dynamic Color-Switching of Plasmonic Nanoparticle Films. *Angew. Chemie* **2019**, *131* (45), 16453–16459. <https://doi.org/10.1002/ange.201910116>.
- (22) Liu, F.; Eisenberg, A. Preparation and PH Triggered Inversion of Vesicles from Poly(Acrylic Acid)-Block-Polystyrene-Block-Poly(4-Vinyl Pyridine). *J. Am. Chem. Soc.* **2003**, *125* (49), 15059–15064. <https://doi.org/10.1021/ja038142r>.
- (23) Shin, S. H. R.; McAninch, P. T.; Henderson, I. M.; Gomez, A.; Greene, A. C.; Carnes, E. C.; Paxton, W. F. Self-Assembly/Disassembly of Giant Double-Hydrophilic Polymersomes at Biologically-Relevant PH. *Chem. Commun.* **2018**, *54* (65), 9043–9046. <https://doi.org/10.1039/c8cc05155k>.
- (24) Dolce, C.; Mériquet, G. Ionization of Short Weak Polyelectrolytes: When Size Matters. *Colloid Polym. Sci.* **2017**, *295* (2), 279–287. <https://doi.org/10.1007/s00396-016-4000-x>.
- (25) Mintis, D. G.; Mavrantzas, V. G. Effect of PH and Molecular Length on the Structure and Dynamics of Short Poly(Acrylic Acid) in Dilute Solution: Detailed Molecular Dynamics Study. *J. Phys. Chem. B* **2019**, *123* (19), 4204–4219. <https://doi.org/10.1021/acs.jpcc.9b01696>.
- (26) Swift, T.; Seaton, C. C.; Rimmer, S. Poly(Acrylic Acid) Interpolymer Complexes. *Soft Matter* **2017**, *13* (46), 8736–8744. <https://doi.org/10.1039/C7SM01787A>.

- (27) Bailey, F. E.; Lundberg, R. D.; Callard, R. W. Some Factors Affecting the Molecular Association of Poly(Ethylene Oxide) and Poly(Acrylic Acid) in Aqueous Solution. *J. Polym. Sci. Part A Gen. Pap.* **1964**, *2* (2), 845–851.  
<https://doi.org/10.1002/pol.1964.100020221>.
- (28) Hao, J.; Yuan, G.; He, W.; Cheng, H.; Han, C. C.; Wu, C. Interchain Hydrogen-Bonding-Induced Association of Poly(Acrylic Acid)- *Graft* -Poly(Ethylene Oxide) in Water. *Macromolecules* **2010**, *43* (4), 2002–2008. <https://doi.org/10.1021/ma9025515>.
- (29) Lakowicz, J. R. *Principles of Fluorescence Spectroscopy*; Springer Science & Business Media, 2006. <https://doi.org/10.1007/978-0-387-46312-4>.
- (30) Selvin, P. R. The Renaissance of Fluorescence Resonance Energy Transfer. *Nat. Struct. Biol.* **2000**, *7* (9), 730–734. <https://doi.org/10.1038/78948>.
- (31) Wu, P. G.; Brand, L. Resonance Energy Transfer: Methods and Applications. *Anal. Biochem.* **1994**, *218* (1), 1–13. <https://doi.org/10.1006/ABIO.1994.1134>.
- (32) Fan, C.; Plaxco, K. W.; Heeger, A. J. Biosensors Based on Binding-Modulated Donor-Acceptor Distances. *Trends in Biotechnology*. April 2005, pp 186–192.  
<https://doi.org/10.1016/j.tibtech.2005.02.005>.
- (33) Bhuckory, S.; Kays, J. C.; Dennis, A. M. In Vivo Biosensing Using Resonance Energy Transfer. *Biosensors* **2019**, *9* (2), 76. <https://doi.org/10.3390/bios9020076>.
- (34) Swift, T.; Paul, N.; Swanson, L.; Katsikogianni, M.; Rimmer, S. Förster Resonance Energy Transfer across Interpolymer Complexes of Poly(Acrylic Acid) and Poly(Acrylamide). *Polym. (United Kingdom)* **2017**, *123*, 10–20.  
<https://doi.org/10.1016/j.polymer.2017.06.069>.
- (35) Hughes, L. D.; Rawle, R. J.; Boxer, S. G. Choose Your Label Wisely: Water-Soluble

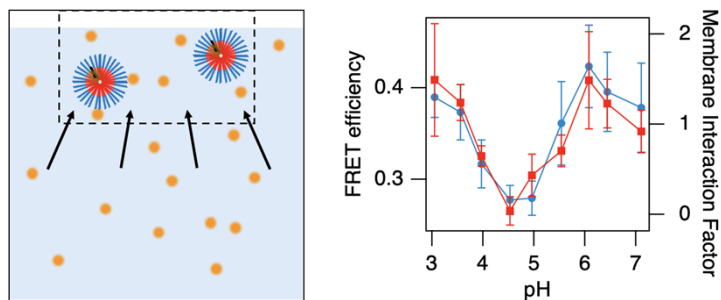
- Fluorophores Often Interact with Lipid Bilayers. *PLoS One* **2014**, *9* (2), e87649.  
<https://doi.org/10.1371/journal.pone.0087649>.
- (36) Van Slyke, D. D. On the Measurement of Buffer Values and on the Relationship of Buffer Value to the Dissociation Constant of the Buffer and the Concentration and Reaction of the Buffer Solution. *J. Biol. Chem.* **1922**, *52* (2), 525–570. [https://doi.org/10.1016/s0021-9258\(18\)85845-8](https://doi.org/10.1016/s0021-9258(18)85845-8).
- (37) PubChem Compound Summary for CID 25137945, Alexa Fluor 594 meta-isomer  
<https://pubchem.ncbi.nlm.nih.gov/compound/Alexa-Fluor-594-meta-isomer> (accessed Apr 6, 2021).
- (38) Urban, V. S. Small-Angle Neutron Scattering. In *Characterization of Materials*; Kaufman, E. N., Ed.; John Wiley & Sons, Inc., 2012.
- (39) Heller, W. T.; Urban, V. S.; Lynn, G. W.; Weiss, K. L.; O'Neill, H. M.; Pingali, S. V.; Qian, S.; Littrell, K. C.; Melnichenko, Y. B.; Buchanan, M. V.; et al. The Bio-SANS Instrument at the High Flux Isotope Reactor of Oak Ridge National Laboratory. *J. Appl. Crystallogr.* **2014**, *47* (4), 1238–1246. <https://doi.org/10.1107/S1600576714011285>.
- (40) Chen, K.; Wang, S.; Guo, X. Confinement Effect on the Aqueous Behaviors of Free Poly(Acrylic Acid) and Poly(Acrylic Acid) Grafted on a Nanoparticle Surface. *Colloid Polym. Sci.* **2019**, *297* (9), 1223–1231. <https://doi.org/10.1007/s00396-019-04541-2>.
- (41) Trachsel, L.; Romio, M.; Grob, B.; Zenobi-Wong, M.; Spencer, N. D.; Ramakrishna, S. N.; Benetti, E. M. Functional Nanoassemblies of Cyclic Polymers Show Amplified Responsiveness and Enhanced Protein-Binding Ability. *ACS Nano* **2020**, *14* (8), 10054–10067. <https://doi.org/10.1021/acsnano.0c03239>.
- (42) Trachsel, L.; Ramakrishna, S. N.; Romio, M.; Spencer, N. D.; Benetti, E. M. Topology

and Molecular Architecture of Polyelectrolytes Determine Their PH-Responsiveness When Assembled on Surfaces. *ACS Macro Lett.* **2021**, *10* (1), 90–97.

<https://doi.org/10.1021/acsmacrolett.0c00750>.

- (43) Förster, T. Zwischenmolekulare Energiewanderung Und Fluoreszenz (Intermolecular Energy Migration and Fluorescence, Translated by Knox RS). *Ann. Phys.* **1948**, *437*, 55–75. <https://doi.org/10.1002/andp.19484370105>.
- (44) Förster, T. 10th Spiers Memorial Lecture Transfer Mechanisms of Electronic Excitation. *Discuss. Faraday Soc.* **1959**, *27*, 7–17. <https://doi.org/10.1039/DF9592700007>.
- (45) Khutoryanskiy, V. V.; Dubolazov, A. V.; Nurkeeva, Z. S.; Mun, G. A. PH Effects in the Complex Formation and Blending of Poly(Acrylic Acid) with Poly(Ethylene Oxide). *Langmuir* **2004**, *20* (9), 3785–3790. <https://doi.org/10.1021/la0498071>.
- (46) Cooper, C. L.; Dubin, P. L.; Kayitmazer, A. B.; Turksen, S. Polyelectrolyte–Protein Complexes. *Curr. Opin. Colloid Interface Sci.* **2005**, *10* (1–2), 52–78. <https://doi.org/10.1016/J.COCIS.2005.05.007>.
- (47) Roth, C. M.; Lenhoff, A. M. Electrostatic and van Der Waals Contributions to Protein Adsorption: Comparison of Theory and Experiment. *Langmuir* **1995**, *11* (9), 3500–3509. <https://doi.org/10.1021/la00009a036>.

### Table of Contents Figure



# Supporting Information

## Complex pH-Dependent Interactions Between Weak Polyelectrolyte

### Block Copolymer Micelles and Molecular Fluorophores

Stacy M. Copp<sup>1,2,3\*</sup>, Ryan L. Hamblin<sup>4†</sup>, Kirstie Swingle<sup>4‡</sup>, Durgesh Rai<sup>5</sup>, Volker Urban<sup>5</sup>, Sergei A. Ivanov<sup>4</sup>, Gabriel A. Montaña<sup>6,7\*</sup>

<sup>1</sup> Department of Materials Science and Engineering, University of California, Irvine, Irvine, CA, 92697-2585, USA

<sup>2</sup> Department of Physics and Astronomy, University of California, Irvine, Irvine, CA, 92697-4575, USA

<sup>3</sup> Department of Chemical and Biomolecular Engineering, University of California, Irvine, Irvine, CA, 92697-2580, USA

<sup>4</sup> Center for Integrated Nanotechnologies, Los Alamos National Laboratories, Los Alamos, NM 87545, USA

<sup>5</sup> Neutron Scattering Division, Oak Ridge National Laboratory, Oak Ridge, ORNL TN 37830, USA

<sup>6</sup> Department of Applied Physics and Materials Science, Northern Arizona University, Flagstaff, AZ, 86011, USA

<sup>7</sup> Center for Materials Interfaces in Research and Applications, Northern Arizona University, Flagstaff, AZ, 86011, USA

\*Co-corresponding authors: stacy.copp@uci.edu, Gabriel.Montano@nau.edu

†Current address: Department of Chemistry, The University of Virginia, Charlottesville, Virginia 22904, USA

‡Current address: School of Molecular Sciences, Arizona State University, Tempe, AZ 85287, USA

#### Table of Contents

Determination of micelle MW, Figure S1	2
Figure S1	2
Figure S2	3
Figure S3	3
SANS details and Figure S4	4-5
Determination of FRET length	6
Figure S5	6
Figure S6	7
Note 1	7
Figure S7	8
Figure S8	8
Figure S9	9
Table S1: Phosphate-Citrate Buffer Composition	9
References	9

### Determination of micelle molecular weight (MW) by static light scattering (SLS)

SLS measurements were performed on a Zetasizer Nano ZS using a 633 nm laser. The following relationship was used to extract the molecular weight:<sup>2</sup>

$$\frac{KC}{R_{\theta}} = \left( \frac{1}{MW} + 2A_2C \right) \quad (S1)$$

K is a physical constant dependent on solvent refractive index, incident light wavelength, and differential refractive index,  $dn/dC$ . C is micelle concentration.  $R_{\theta}$  is the excess Rayleigh ratio.  $A_2$  is the second virial coefficient.

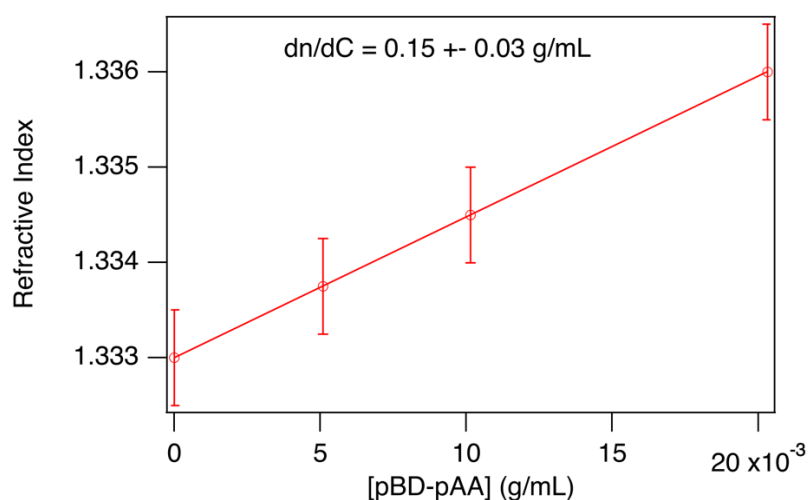


**Figure S1:** Refractive index as a function of pBD-pAA concentration. The differential refractive index,  $dn/dC$ , is determined by linear least-squares fitting. Error bars represent the finest degradations on the Abbe-3L refractometer.

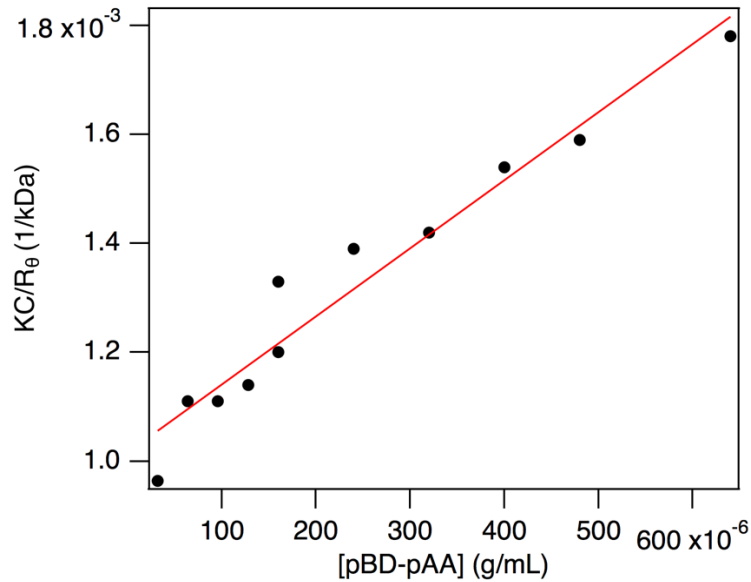


**Figure S2:** Experimentally measured  $KC/R_{\theta}$  as a function of micelle concentration, as measured by SLS (black markers) on a Zetasizer Nano ZS with fixed backscatter angle of  $173^{\circ}$ . Linear least squares fit to data (red line) is used to extract the micelle MW.

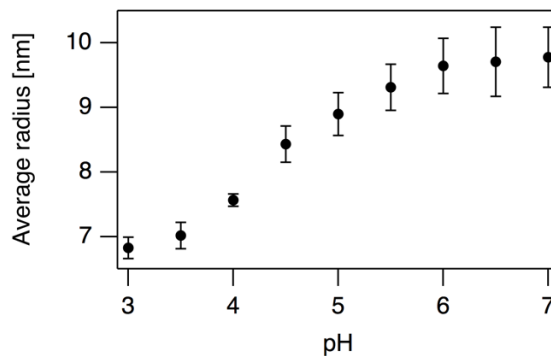


**Figure S3:** Radius of pBD-pAA micelles, as determined by dynamic light scattering (DLS). Radii are determined from the volume distribution. To convert from intensity distribution to volume distribution, the refractive index of the micelles was approximated by the average refractive index of pBd and pAA weighted by MW. The reader should note that the refractive index of pAA is likely to decrease with pH as hydration increases, making conversion to volume distribution less accurate for particles with sizes comparable to the wavelength of light. Because the pBd-pAA micelles are much smaller in diameter than the 633 nm laser light used here, the conversion of intensity distribution to volume distribution using Mie theory will be only negligibly impacted by any variations in micelle refractive index.

**Small Angle Neutron Scattering (SANS):** A core-shell sphere model accounting for polydispersity was used to analyze SANS data. The scattering intensity from dilute vesicles using a poly-core-shell model is given by:

$$I(q) = A \left[ \sum_{i=1}^2 \frac{3V_i(\rho_i - \rho_{i-1})j_1(qd_i)}{qd_i} \right]^2 + bkg$$

where  $A$  is the scaling factor,  $bkg$  the  $q$ -independent background,  $V_i$ ,  $d_i$  and  $\rho_i$  the volume, thickness and scattering length density respectively, of core and shells. The subscripts  $i=1,2$  represent the core and shell regime respectively.  $j_1(x)$  is the first order Bessel function. The size-distribution (polydispersity) of micelles is accounted for in the model using the Schulz distribution function for the core thickness (or radius):<sup>3</sup>

$$s(d) = \left( \frac{z+1}{d_m} \right)^{z+1} d^z \frac{\exp\left\{ \left( \frac{z+1}{d_m} \right) d \right\}}{\Gamma(z+1)}$$

where  $d_m$  is the mean radius of the polydisperse core,  $z = \frac{1}{(PDI)^2} - 1$ , and  $PDI$  is the

polydispersity index. Using the  $n^{th}$  moment of size distribution,

$$\langle d^n \rangle = \frac{d_m^n}{(z+1)^n} \frac{(z+n)!}{z!},$$

the core volume *via* 3<sup>rd</sup> moment of size distribution is evaluated as:

$$\langle V \rangle = \frac{4\pi}{3} \langle d^3 \rangle = \frac{4\pi}{3} \frac{d_m^3}{(z+1)^3} \frac{(z+3)!}{z!} = \frac{4\pi}{3} \frac{d_m^3 (z+3)(z+2)}{(z+1)^2}$$

Polydispersity is not implemented on the shell thickness.

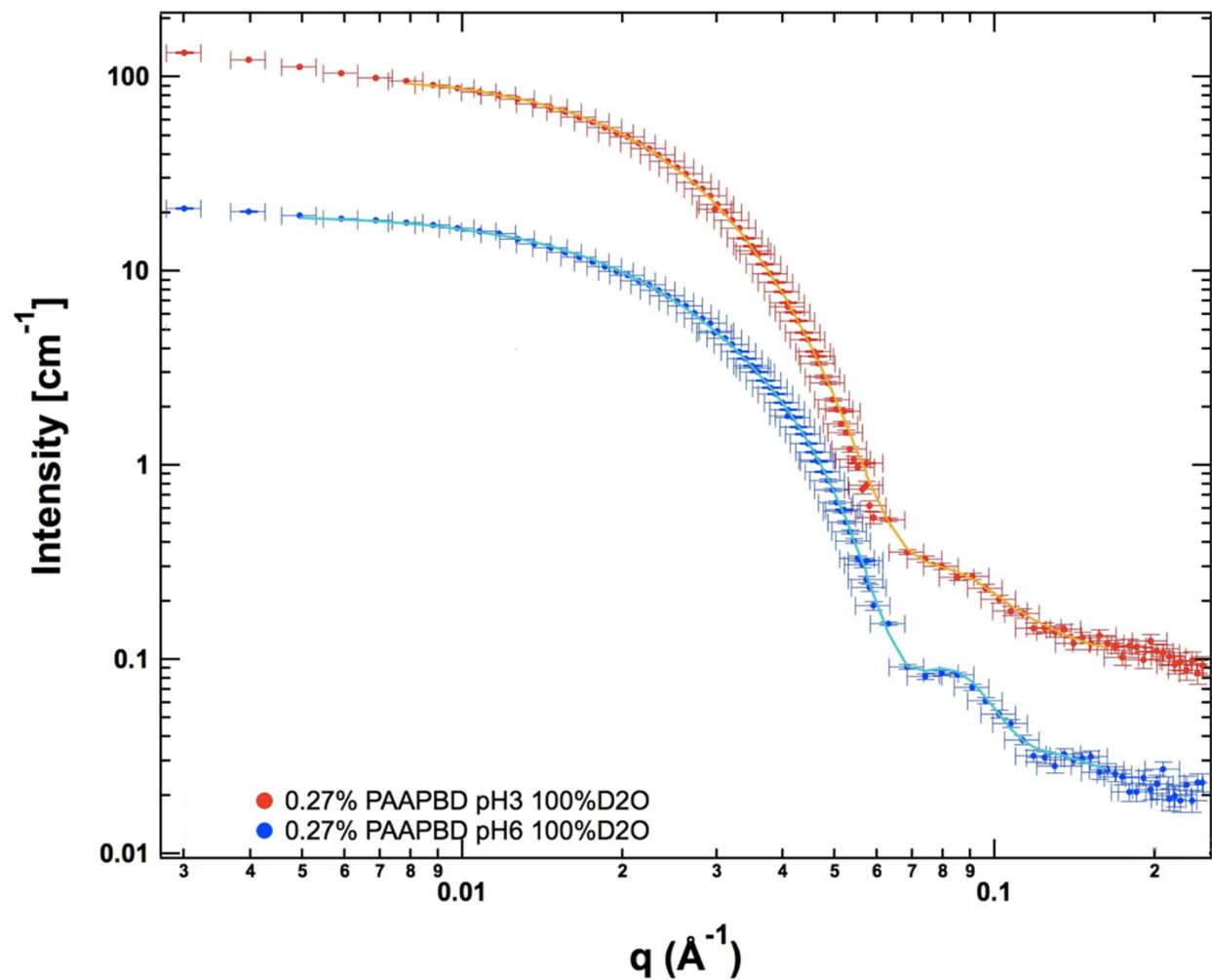


**Figure S4:** Small angle neutron scattering intensity as a function of scattering vector magnitude  $q$ . Data points shown with statistical error bars (counting statistics in intensity and FWHM resolution in  $q$ ); solid lines are fits with the core-shell sphere model.

## Determination of FRET length

The characteristic FRET length,  $R_0$ , is defined as follows:

$$R_0^6 = \frac{9 \ln 10}{128\pi^5 N_A} \cdot \frac{Q_0 \kappa^2}{n^4} \int F_D(\lambda) \cdot \epsilon_A(\lambda) \cdot \lambda^4 \cdot d\lambda \quad (\text{S1})$$

Where  $N_A$  is Avogadro's number,  $Q_0$  is the quantum yield of the donor,  $n$  is the medium refractive index,  $\kappa$  is a factor dependent on relative orientations of donor and acceptor fluorophores (here  $\kappa^2 = 2/3$ , corresponding to the assumption that fluorophores are free to rotate and are thus isotropically distributed),  $F_D(\lambda)$  is the emission spectrum of the donor normalized to  $\int F_D(\lambda) \cdot d\lambda = 1$ , and  $\epsilon_A(\lambda)$  is the molar extinction coefficient.

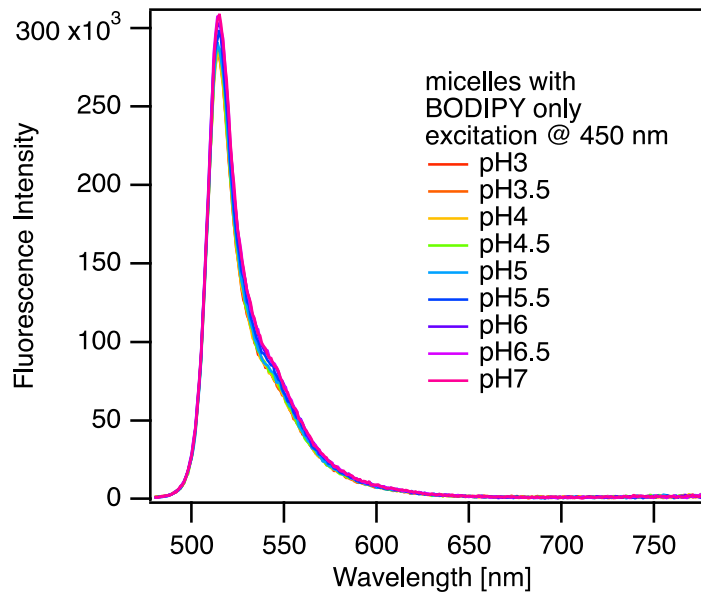


**Figure S5: Dependence of BODIPY fluorescence emission on pH.** Fluorescence emission from pBd-pAA micelles containing BODIPY-HPC and in the absence of any acceptor dye. Changes in pH induce a slight change in the intensity but not spectral shape of the fluorescence emission, with fluorescence emission increased by  $8 \pm 3\%$  at high pH values compared to the fluorescence emission at low pH (average and standard deviation determined by triplicate experiments).

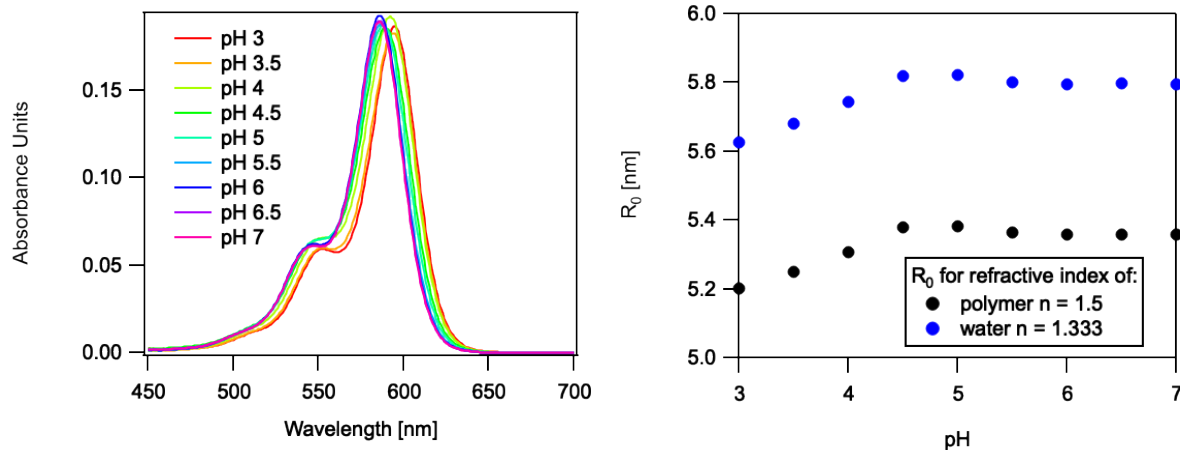


**Figure S6:** Left: Fluorescence intensity of 2  $\mu\text{M}$  Alexa 594 (A594) in phosphate-citrate buffer at varying pH, as annotated by color specified in figure legend. Right: Calculated FRET length,  $R_0$ , for a BODIPY donor and A594 acceptor as a function of pH, using the experimentally measured absorbance spectra in the left graph. As specified in the main text, because the medium separating donor and acceptor is composed of both water and pAA, calculations are presented for both refractive indices in the legend. The slight pH-induced shifts in A594 result in a shift of about 0.2 nm in  $R_0$ .

#### Note 1: Calculation of micelle corona expansion volume

We calculate the volume expansion of the pAA-pBd micelle from pH 3 to pH 6. For micelle pBd core radius  $r_i$  and pAA shell thickness  $S_i$ , the change in volume is given by:

$$\Delta V = \frac{4}{3} \pi [(r_2 + S_2)^3 - (r_1 + S_1)^3]$$

Subscript  $i=1$  represents pH 3, and  $i=2$  represents pH 6. Using dimensions determined by SANS (Table 1 main text),  $\Delta V = 8,200 \text{ nm}^3$ . Because the change in pAA corona is much greater than the change in the pBd core for increased pH, we estimate that  $\Delta V$  corresponds to the change in pAA corona volume upon deprotonation and swelling of the pAA with additional waters.

Next, we estimate the increase in the number of A594 acceptors which would be expected to occupy this  $8,200 \text{ nm}^3$  volume increase if A594 are uniformly distributed throughout solution and solvated pAA chains. The concentration of A594 in Figure 3 of the main text was  $1.4 \mu\text{M}$ , corresponding to  $8.4 \times 10^{-7} \text{ A594 molecules/nm}^3$ . Thus, within the  $8,200 \text{ nm}^3$  of increased water content of the pAA micelle corona, we expect  $(8.4 \times 10^{-7} \text{ nm}^{-3}) \cdot (8,200 \text{ nm}^3) = 0.007 \text{ A594 molecules per micelle}$ .

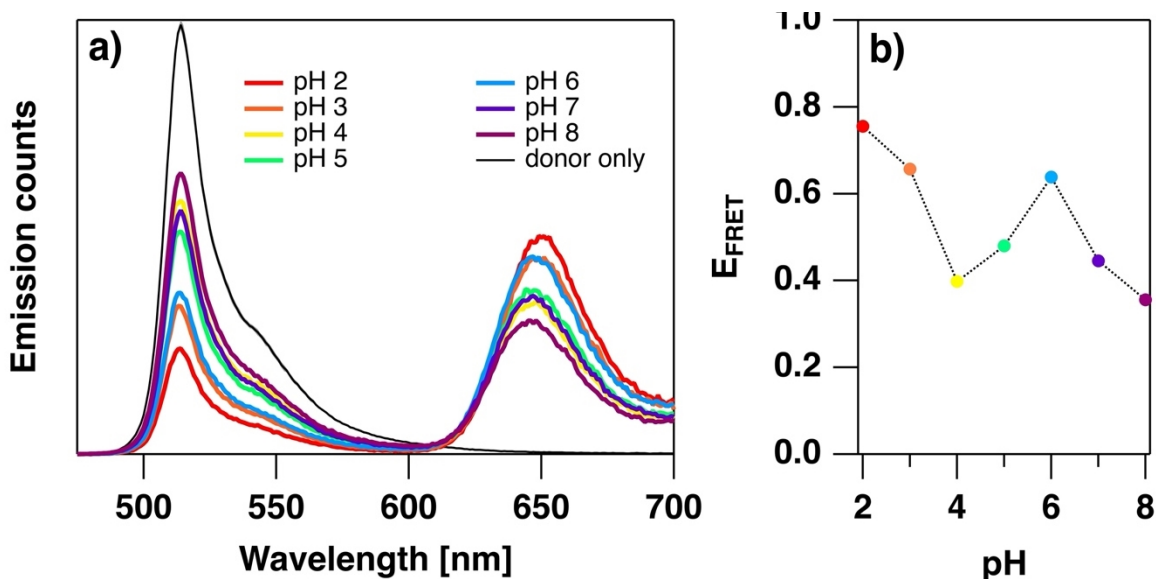


**Figure S7:** a) Raw emission spectra and b) calculated  $E_{FRET}$  for solutions of micelles with BODIPY-HCP donors and AlexaFluor 633 acceptors, using a universal buffer system with expanded pH range as compared to the phosphate/citrate buffer system used for the main studies here.

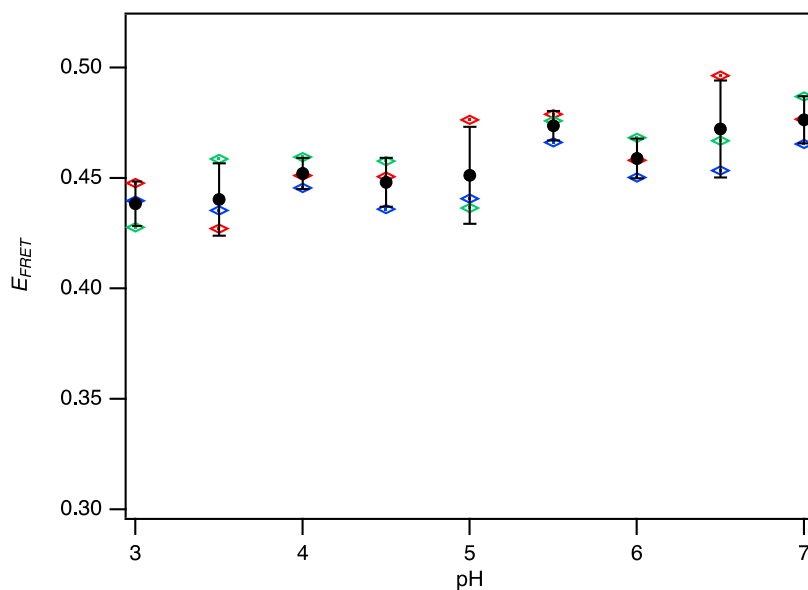


**Figure S8:**  $E_{FRET}$  values for pBd-pAA micelles with donors and acceptors embedded within the micelle: BODIPY-HCP donors and Texas Red DHPE acceptors. Average and standard deviation (black dots and brackets) are based on triplicate experiments, with individual values shown in red, green, and blue diamonds. Axis range is set to same magnitude as Figure 3b of main text to enable direct comparison.

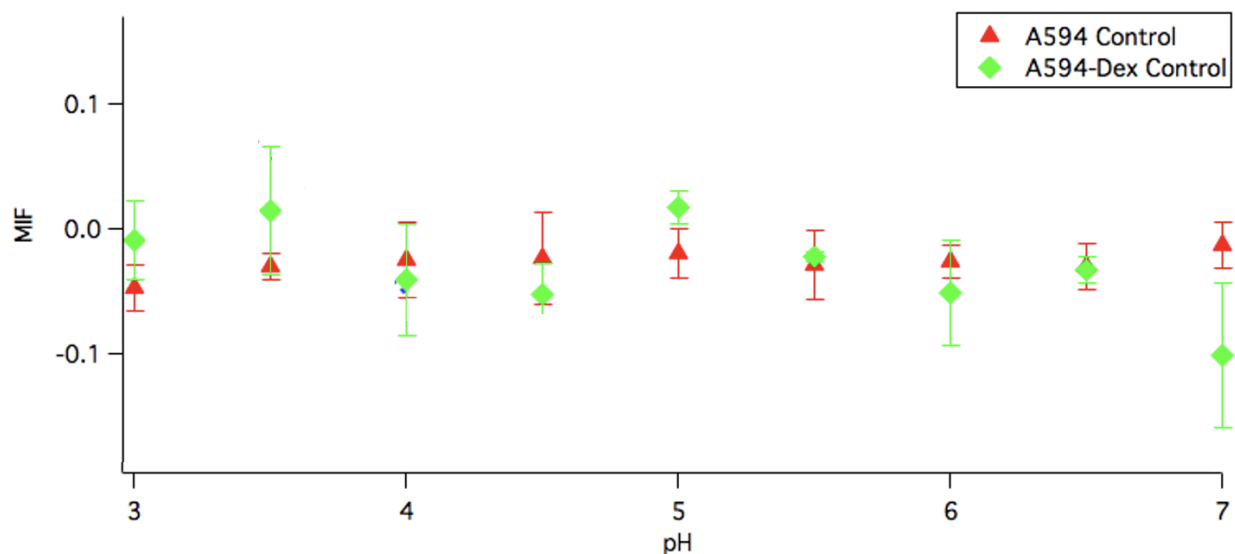


**Figure S9:** *MIF* as a function of pH for A594 and A594-dextran in the absence of pBd-pAA micelles, showing that *MIF* is approximately zero for all cases studied.

Na <sub>2</sub> HPO <sub>4</sub> (g/100 mL)	Sodium Citrate (g/100 mL)	pH
0.87	3.51	3.0
1.29	3.08	3.5
1.64	2.71	4.0
1.94	2.40	4.5
2.19	2.14	5.0
2.42	1.91	5.5
2.73	1.58	6.0
3.02	1.28	6.5
3.71	0.57	7.0

**Table S1: Phosphate-Citrate Buffer Composition.** Buffer composition table for phosphate-citrate buffer used in scattering and spectroscopy experiments. Disodium hydrogen phosphate and trisodium citrate dihydrate were utilized as the phosphate and citrate sources respectively. Indicated masses of each reagent were combined with molecular biology reagent-grade water for 100mL buffer solution.

## References

- 1 PubChem Compound Summary for CID 25137945, Alexa Fluor 594 meta-isomer, <https://pubchem.ncbi.nlm.nih.gov/compound/Alexa-Fluor-594-meta-isomer>, (accessed 6 April 2021).
- 2 P. J. Wyatt, *Anal. Chim. Acta*, 1993, 272, 1–40.
- 3 G. V. Schulz, *Zeitschrift für Phys. Chemie*, 1935, **30**, 379.